

Hydroxypyridinone Functionalized Self-Assembled Monolayers on Nanoporous Silica for Sequestering Lanthanide Cations

Wassana Yantasee,¹ Glen E. Fryxell,^{1,*} Yuehe Lin,¹
Hong Wu,¹ Kenneth N. Raymond,² and Jide Xu²

¹Pacific Northwest National Laboratory, Richland, Washington 99352, USA

²Department of Chemistry, University of California at Berkeley,
Berkeley, California 94720-1460, USA

1,2-Hydroxypyridinone (1,2-HOPO) ligands were installed as self-assembled monolayers on nanoporous silica (MCM-41) to create a superior class of sorbent materials for lanthanide cations. Lanthanides were used as a model system for the radioactive, expensive, and highly hazardous actinides in preliminary screening studies. The ligand properties of the 1,2-HOPO ligand field and the extremely large surface area of MCM-41, coupled with the dense monolayer coating, contribute to the extremely high lanthanide binding capacity of the 1,2-HOPO nanoporous sorbent. At pH 4–5.9, the mass-weighted partition coefficients (K_d) for La, Nd, Eu, and Lu were 354 000, 344 000, 210 800, and 419 800, respectively. The rigid, open pore structure of the silica also allows for very rapid sorption. Being silica-based, the sorbent is compatible with vitrification processing into a final glassy waste form, for subsequent disposition in a deep geological repository.

Keywords: MCM-41, 1,2-Hydroxypyridinone, Nanoporous Silica, Lanthanides.

Long-lived radioactive actinide species resulting from 40 years of plutonium production are present at very low concentrations in millions of gallons of DOE legacy wastes. Selective removal of these species could greatly reduce the volume of materials to be subsequently vitrified for long-term storage. To be effective for removing low level actinides from tank wastes, the adsorbent must be selective for the target species among other interfering cations and/or competing ligands.

Rare earth cations are hard Lewis acids, that are considerably larger than the typical transition-metal cations,¹ thus both hard anionic ligands and ligand synergy are important attributes in designing effective complexing agents for these species. The hydroxypyridonates (HOPO)^{2–7} are highly selective f-block chelators, inspired by iron binding siderophores from bacteria. The HOPO ligands have been synthesized and evaluated as liquid–liquid extractants for both *in-vivo* actinide decorporation^{8–10} and nuclear waste remediation.^{11–13} A very important feature of the HOPO

ligands is the strong hydrogen bond formed between the amide proton and the adjacent phenolic oxygen in the metal complex, thereby enhancing the stability of the metal–ligand complex.² This feature stabilizes the 1,2-HOPO complexes. The 1,2-HOPO ligand has the lowest protonation constant among the three HOPO ligands¹² and thus under acidic conditions should have the highest affinity for lanthanides. For this reason, the 1,2-HOPO ligand was chosen for these preliminary trials.

Self-assembled monolayers on nanoporous silica (MCM-41) have been developed as high-performance sorbent materials (Fig. 1) whose functional groups can be tailored to selectively sequester many target species.^{14–21} The high surface area of the nanoporous support, coupled with the dense monolayer coating, provides high binding capacity. The rigid, open pore structure allows for rapid sorption kinetics. This manuscript describes the synthesis and performance of a new class of sorbent material designed to selectively bind rare earth cations, achieved by combining the HOPO ligands with nanoporous silica materials.

In order to evaluate the efficacy of HOPO on nanoporous silica, we prepared 1,2-HOPO terminated silanes

*Author to whom correspondence should be addressed.

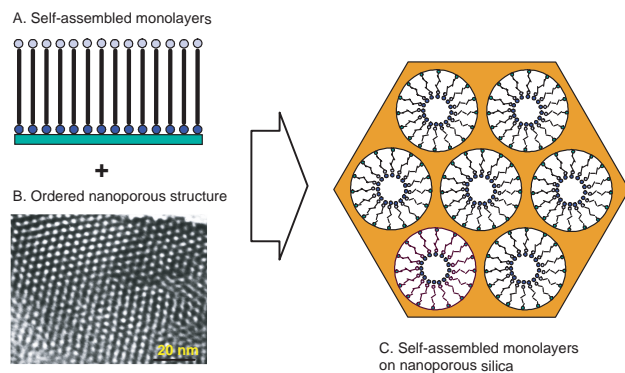
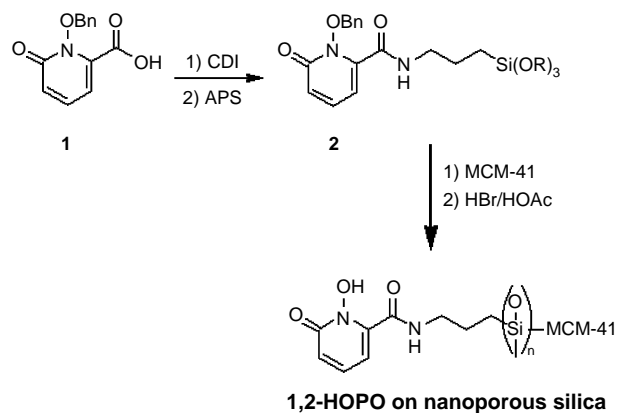


Fig. 1. Self-assembled monolayers on nanoporous silica (MCM-41).

and incorporated them into a nanoporous silica (MCM-41) framework.¹⁴ Since the actinides are radioactive, expensive, and hazardous to work with, we chose to perform preliminary screening studies using lanthanides as a model system: La(III) as a “light” lanthanide that has an ionic radius very similar to Th(IV),¹ Nd(III) as a “typical” lanthanide with an ionic radius similar to many of the actinide cations, Eu(III) as an Am(III) mimic and because it has very similar in size to U(IV), Np(IV), and Pu(IV),¹ and, finally, Lu(III) because it has an ionic radius between those of rare earth cations and transition-metal cations.

MCM-41 was prepared as described previously¹⁴ and was characterized by XRD, BET, and solid state ²⁹Si NMR. The MCM-41 was found to have 65-Å pores, to have a surface area of 880–900 m²/g, to be composed of a well-crosslinked SiO₂ backbone, and to be disordered. The self-assembled monolayers were deposited in MCM-41 by carefully prehydrating the ceramic with approximately 2–2.5 monolayers worth of water (approximately 0.32 mL of water for each 1.0 g of MCM-41), followed by treatment with a slight (ca. 10–15%) excess of silane (relative to available surface area), and the mixture was held at toluene reflux for 4–6 h. The mixture was then cooled to ambient temperature and filtered and the collected solid washed copiously with 2-propanol. The SAMMS were then air-dried to constant weight in a fume hood and characterized by using solid-state ²⁹Si and ¹³C NMR and BET. In general, the coated materials display surface area to mass ratios that are approximately half of the original MCM-41 surface area, due to the added weight of the ligand/silane and the reduced surface area caused by pore filling.

The silane synthesis started off with the benzyl-protected HOPO acid (**1**) (1,2-HOPOBn-6-carboxylic acid).^{2–7,9} The chemistry involved in anchoring the HOPO ligand onto MCM-41 is summarized in Figure 2.^{22,23} The benzyl-protected HOPO acid (**1**, 0.5 g) was dissolved in 25 mL of anhydrous DMF (under dry N₂) and treated with 1.0 equiv of carbonyldiimidazole (CDI). After cessation of CO₂ evolution (about 20 min), 1.0 equiv (0.36 g) of freshly distilled (3-aminopropyl)trimethoxysilane (APS) was added. The resulting solution was stirred at ambient temperature under N₂ for at least 4 h. While the silane



1,2-HOPO on nanoporous silica

Fig. 2. CDI mediated silane coupling reactions for attachment of HOPO moieties onto nanoporous silica.

solution was stirring, a 0.68-g sample of MCM-41 was suspended in 25 mL of toluene and treated with 0.21 mL of water (approximately 2 monolayers). This suspension was then stirred for 2 h to make sure that the water was uniformly distributed throughout the nanoporous matrix. At the end of this pretreatment, the silane (**2**) solution described above was added to the MCM-41 suspension. This solution was then taken to reflux for 6 h. After this period, it was cooled to ambient temperature, filtered, washed with isopropanol, and air-dried. Deprotection was accomplished by treating the benzylated 1,2-HOPO on nanoporous silica with 10% HBr in acetic acid and stirring the suspension overnight at ambient temperature. The product was collected by filtration, washed with isopropanol, and air-dried. Removal of the benzyl protecting group was confirmed by solid-state ¹³C NMR.

Lanthanide adsorption studies were performed in batch contact mode by adding a known quantity of the 1,2-HOPO on nanoporous material into the multicomponent lanthanide solutions of 2 mg/L (each) of La³⁺, Lu³⁺, Nd³⁺, and Eu³⁺ in diluent containing 0.1 M NaNO₃/0.05 M CH₃CO₂Na (nominal pH varied from 2 to 6). The solution to solids ratio was held constant at 200.

Table I summarizes the distribution coefficient (*K_d*) values of 1,2-HOPO on nanoporous silica for selected lanthanides. In 0.1 M nitrate and 0.05 M acetate solution at pH 5.9, the *K_d* values for La, Nd, Eu, and Lu were

Table I. Distribution coefficient (*K_d*) values of 1,2-HOPO on nanoporous silica for selected lanthanides.

Medium	La	Nd	Eu	Lu
0.1 M NaNO ₃ /0.05 M NaAc (pH = 5.9)	354 000	344 000	210 800	419 800
0.1 M NaNO ₃ /0.05 M NaAc (pH = 4.0)	367 600	353 800	139 800	421 800
0.1 M NaNO ₃ /0.05 M NaAc (pH = 1.9)	220	1041	1444	14729
0.1 M HNO ₃	19	29	39	133
1.0 M HNO ₃	3	0	0	0
3.0 M HNO ₃	12	7	0	0

354 000, 344 000, 210 800, and 419 800, respectively. The distribution coefficient is simply a mass-weighted partition coefficient. A K_d value of 354 000 for Lu means that for a solution to solids ratio of 200, there was 1770 times as much Lu in the 1,2-HOPO on nanoporous silica as was left in the residual supernatant at equilibrium. Such high K_d values indicate the very high affinity that the 1,2-HOPO on nanoporous silica has for the lanthanide cations. The K_d values remained relatively stable even when the solution pH decreased from 5.9 to 4.0. At pH's below 1, the binding affinity of 1,2-HOPO on nanoporous silica for these lanthanide cations dropped off to essentially zero. These results indicate that the lanthanides can be stripped from the 1,2-HOPO on nanoporous silica and the sorbent material regenerated, using a simple acid strip.

The 1,2-HOPO on nanoporous silica is a highly efficient adsorbent for lanthanides and actinides because the relatively close proximity of the HOPO ligands on the silica surface allows for multiple ligand/metal interactions once the metal species is bound to the first HOPO ligand. NMR analysis reveals that the ligand population density is approximately 0.5–1 silane/nm², and each silane is approximately 1.2 nm long. Therefore, it is possible for two, three, or even four ligands to bind a single metal cation in these systems. This macromolecular chelation provides an additional driving force for sequestering the rare earth species inside the nanoporous matrix.

In addition to the superior HOPO ligand fields, the honeycomb structure of the MCM-41 support provides a rigid, uniform wall structure that does not undergo solvent swelling as do polymer-based ion-exchange resins (solvent-swelling can close off pores, making portions of the resin inaccessible). As a result, the sorption kinetics of nanoporous silica materials is generally very rapid.²¹

The high binding affinity for the various lanthanide cations used in this study suggests that HOPO on nanoporous silica should be of value in binding virtually all actinide cations, regardless of ionic radius, making them of real value for cleaning up radioactive waste. These materials are also intended to be applied in complex aqueous mixtures (preferably homogeneous solutions, but not limited to them) containing heavy metals or radionuclides. They are particularly well-suited to applications in acidic media, are effective down to a pH of 0, and are stable up to a pH of about 9. Evaluation of HOPO on nanoporous silica for actinide separations will be reported in due course.

The efficient chemical separations afforded by HOPO on nanoporous silica avoids secondary wastestreams produced by other lanthanide/actinide separation processes (e.g., solvent extraction). Also, being silica-based, this class of materials is compatible with vitrification processing into a final glassy waste form, for subsequent disposition in a deep geological repository.

Acknowledgments: This research was supported by the U.S. Department of Energy (DOE), Environmental Management Science Program. Portions of this work were performed at Pacific Northwest National Laboratories, which is operated for the DOE by Battelle Memorial Institute under contract DE AC06-76RLO 1830. The work at LBNL was partially supported by the Office of Energy Research, Office of Basic Energy Sciences, Chemical Sciences Division, U.S. Department of Energy, under contract number DE-AC03-76F00098.

References and Notes

1. Ionic radii (in Å) of representative lanthanides, La(III) 1.016, Nd(III) 0.995, Eu(III) 0.95, Lu(III) 0.85, compared to those of actinides, Th(IV) 1.02, U(IV) 0.97, Pu(IV) 1.08, Am(III) 1.07, and some common transition metal cations, Cu(II) 0.72, Fe(III) 0.64, Ni(II) 0.69, Zn(II) 0.74. The values were taken from: *CRC Handbook of Chemistry and Physics*, Boca Raton, FL, 60th ed., pp. F214–F215 (1979).
2. A. E. V. Gordon, J. Xu, K. N. Raymond, and P. W. Durbin, *Chem. Rev.* 103, 4207 (2003).
3. J. Xu, D. W. Whisenhunt, Jr., A. C. Veeck, L. C. Uhlir, and K. N. Raymond, *Inorg. Chem.* 42, 2665 (2003).
4. J. Xu, P. W. Durbin, B. Kullgren, S. N. Ebbe, L. C. Uhlir, and K. N. Raymond, *J. Med. Chem.* 45, 3963 (2002).
5. J. Xu, E. Radkov, M. Ziegler, and K. N. Raymond, *Inorg. Chem.* 39, 4156 (2000).
6. P. W. Durbin, B. Kullgren, J. Xu, K. N. Raymond, M. H. Hengè-Napoli, T. Bailly, and R. Burgada, *Rad. Prot. Dosim.* 105, 503 (2003).
7. R. A. Guilmette, R. Hakimi, P. W. Durbin, J. Xu, and K. N. Raymond, *Rad. Prot. Dosim.* 105, 527 (2003).
8. D. L. White, P. W. Durbin, N. Jeung, and K. N. Raymond, *J. Med. Chem.* 31, 11 (1988).
9. J. Xu, B. Kullgren, P. W. Durbin, and K. N. Raymond, *J. Med. Chem.* 38, 2606 (1995).
10. J. Xu and K. N. Raymond, *Inorg. Chem.* 38, 308 (1999).
11. D. W. Whisenhunt, Jr., M. P. Neu, Z. Hou, J. Xu, D. C. Hoffman, and K. N. Raymond, *Inorg. Chem.* 35, 4128 (1996).
12. V. V. Romanovski, D. White, J. Xu, D. C. Hoffman, and K. N. Raymond, *Solvent Extr. Ion Exch.* 17, 55 (1999).
13. P. H. Zhao, V. V. Romanovski, D. W. Whisenhunt, D. C. Hoffman, T. R. Mohs, J. Xu, and K. N. Raymond, *Solvent Extr. Ion Exch.* 17, 1327 (1999).
14. X. Feng, G. E. Fryxell, L. Q. Wang, A. Y. Kim, J. Liu, and K. Kemner, *Science* 276, 923 (1997); J. Liu, X. Feng, G. E. Fryxell, L. Q. Wang, A. Y. Kim, and M. Gong, *Adv. Mater.* 10, 161 (1998).
15. S. V. Mattigod, G. E. Fryxell, R. J. Serne, K. E. Parker, and F. M. Mann, *Radiochim. Acta* 91, 539 (2003).
16. J. C. Birnbaum, B. Busche, W. Shaw, and G. E. Fryxell, *Chem. Commun.* 1374 (2002).
17. Y. Lin, G. E. Fryxell, H. Wu, and M. Englehard, *Envi. Sci. Technol.* 35, 3962 (2001).
18. T. S. Zemanian, G. E. Fryxell, J. Liu, J. A. Franz, and Zimin Nie, *Langmuir* 17, 8172 (2001).
19. G. E. Fryxell, J. Liu, M. Gong, T. A. Hauser, Z. Nie, R. T. Hallen, M. Qian, and K. F. Ferris, *Chem. Mat.* 11, 2148 (1999).
20. S. V. Mattigod, X. Feng, G. E. Fryxell, J. Liu, and M. Gong, *Sep. Sci. Technol.* 34, 2329 (1999).
21. W. Yantasee, Y. Lin, G. E. Fryxell, B. J. Busche, and J. C. Birnbaum, *Sep. Sci. Technol.* 38, 3809 (2003).

Received: 27 September 2004. Revised/Accepted: 3 November 2004.

Doping of Si into GaN Nanowires and Optical Properties of Resulting Composites

Congkang Xu,¹ Sangyong Chung,¹ Misuk Kim,¹ Dong Eon Kim,^{1,*}
Bonghwan Chon,² Sangsu Hong,² and Taiha Joo^{2,*}

¹Department of Physics and Electron Spin Science Center, ²Department of Chemistry,
Pohang University of Science and Technology, Pohang 790-784, South Korea

Doping of Si into GaN nanowires has been successfully attained via thermal evaporation in the presence of a suitable gas atmosphere. Analysis indicated that the Si-doped GaN nanowire is a single crystal with a hexagonal wurtzite structure, containing 2.2 atom % of Si. The broadening and the shift of Raman peak to lower frequency are observed, which may be attributed to surface disorder and various strengths of the stress. The band-gap emission (358 nm) of Si-doped GaN nanowires relative to that (370 nm) of GaN nanowires has an apparent blue shift (~12 nm), which can be ascribed to doping impurity Si.

Keywords: GaN Nanowires, Raman Scattering, Photoluminescence, Nanocomposites.

Recently, the fabrication and properties of nanometer-sized materials such as GaN nanowires (NWs) have attracted considerable attention owing to their potential applications in both testing the fundamental concept of quantum mechanics and the development of nanodevices.^{1–5} So far, many techniques have been developed for the synthesis of pure GaN NWs such as laser ablation,^{6,7} thermal chemical vapor deposition (CVD),^{8–13} arc discharge,¹⁴ nanotube-confined reaction,¹⁵ and anodic alumina templates (AAO).¹⁶ In order to exploit the practicable applications, it is of much importance and significance to tailor the properties of pure GaN NWs by doping special elements such as manganese, cobalt, and silicon. The former elements (Mn, Co) can introduce their magnetic properties to GaN NWs (diluted magnetic semiconductors); the latter may modify the conductivity and photoluminescence of GaN NWs. However, only a few experiments have been performed.^{17,18} Theoretically, it has been reported that Si atoms residing in Ga sites in GaN are neutral shallow donors.¹⁹ Thus, the Si-doped GaN nanowires are expected to have interesting electronic properties. This point attracts our scientific interest and is also needed for their future applications. Little work on doping of Si into

GaN nanowires has been done to date; a simple and effective approach for the preparation of the nanowires remains a challenge. In this paper, we present single-crystalline Si-doped GaN nanowires and GaN nanowires via a simple route in the absence of template¹⁷ and catalyst such as Au.¹⁸ Si-doped GaN and undoped GaN NWs are synthesized through the reaction of high purity Ga₂O₃ powders with NH₃ and Ar 95% + H₂ 5% in a furnace. The growth mechanisms of GaN based nanowires are discussed.

A quartz boat containing reagent-grade Ga₂O₃ powder (Aldrich, 99.99%) was kept in the center of a quartz tube placed horizontally in a tubular furnace as shown in Figure 1a. Cleaned SiO₂ substrates were placed downstream from the boat. The distances between the boat and substrates were 25 (A) and 30 cm (B), respectively. The base vacuum was kept at 95 mTorr. The powder was heated up to 900 °C at the rate of 15 °C/min with a flow of Ar 95% + H₂ 5% at a rate of 60 sccm, Ar + H₂ gas was then turned off, and a pure ammonia gas (99.999%) was introduced at a rate of 150 sccm. The furnace was then heated up to 1080 °C at the rate of 10 °C/min and maintained for 160 min. The pressure was kept at 675 Torr. The temperature distribution is shown in Figure 1b. After the furnace was cooled with NH₃, the samples were taken from the substrates.

*Author to whom correspondence should be addressed.

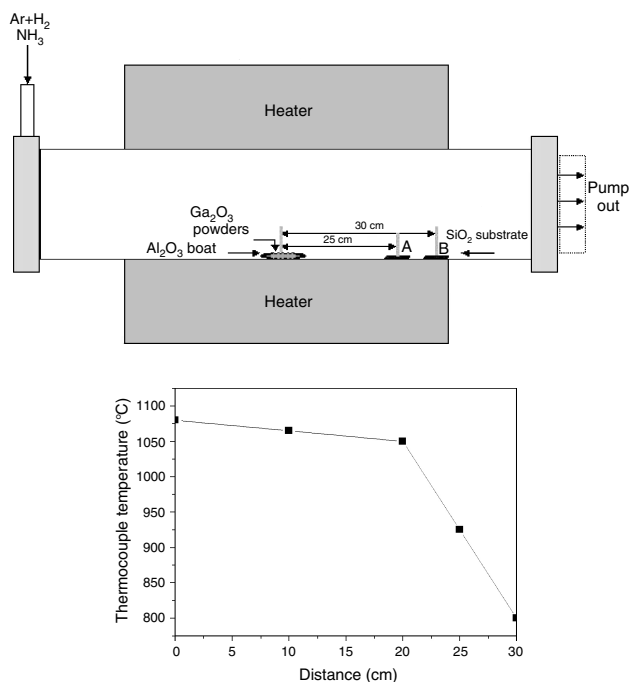


Fig. 1. (a) Schematic diagram of the horizontal furnace used in the synthesis. (b) The temperature distribution curve in the furnace.

The as-prepared samples were investigated by X-ray diffraction (XRD, Rigaku D/max-rB $\text{Cu K}\alpha$). The morphology and size distribution of the nanowires were characterized with a scanning electron microscope (SEM, Hitachi H-8010) equipped with an energy-dispersive X-ray (EDX) spectrometer and a transmission electron microscope (TEM, Hitachi H-800). High-resolution TEM (HRTEM), EDX and electron diffraction (ED) analysis were performed with JEOL-2010. The Raman backscattering measurements were performed at room temperature using a Spex 1403 Raman scattering spectrometer and a 200 mW Ar^+ laser at 488 nm as the excitation source. The third harmonic of a cavity-dumped femtosecond Ti:sapphire laser at 266 nm was used as an excitation source in the photoluminescence (PL) measurement.

Wool-like products on SiO_2 substrates appear in two distinguished colors. Typical SEM images of the sample A and B are shown in parts a and b of Figure 2, respectively. Sample A formed on substrate A at 25 cm (around 900–950 °C) downstream from the target materials is deep gray, whereas sample B formed on substrate B at 30 cm (around 800 °C) is light yellow. The boundary between these two regions was quite sharp. The diameters of the nanowires in sample A range from 50 to 200 nm, and the length is up to a few micrometers. The diameters of the nanowires in the sample B range from 50 to 450 nm. Statistic analyses indicate that the number of larger diameter nanowires in sample B is greater than that in sample A.

Figure 3 illustrates XRD of the as-prepared sample A and B. As shown in Fig. 3(a), the diffraction peaks in sample A are quite similar to those of a bulk GaN,

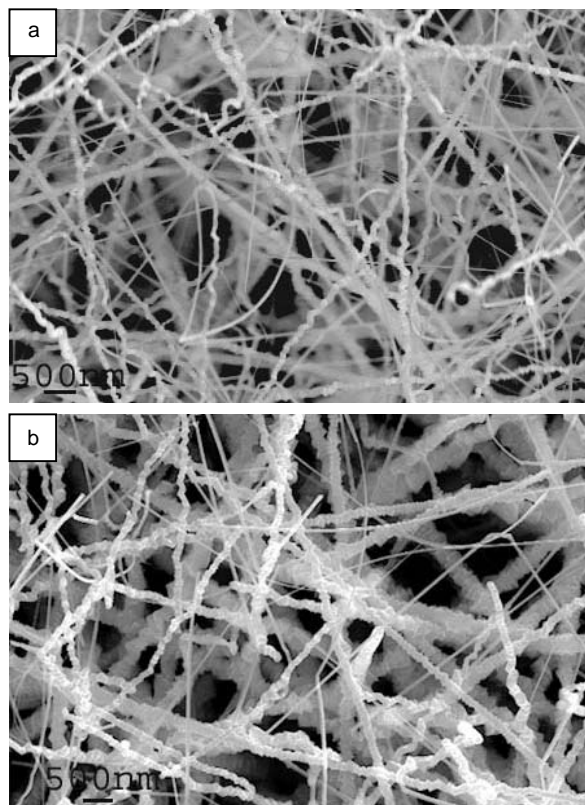


Fig. 2. Typical SEM images of the samples A (a) and B (b).

which can be indexed to (100), (002), (101), (102), (110), (103), (200), (112), (201), and (004) of hexagonal wurtzite structure GaN ($a = 3.18 \text{ \AA}$, $c = 5.18 \text{ \AA}$). The diffraction data are in good agreement with published values⁹ for GaN nanowires. No obvious diffraction peak corresponding to Si or Si compound impurity phases is observed. The peak (002) is the strongest, and other peaks are relatively weak. The strong intensities of the peaks relative to the background delineate that the nanowires are well-crystallized. However, the diffraction peaks of the sample B (Fig. 3b)

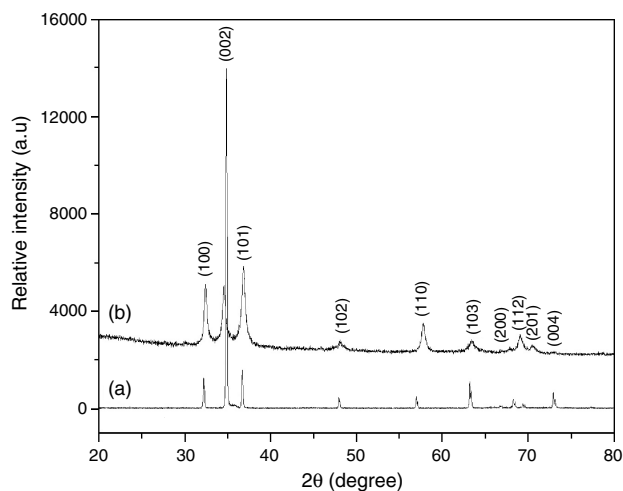


Fig. 3. XRD pattern of the as-prepared samples A (a) and B (b).

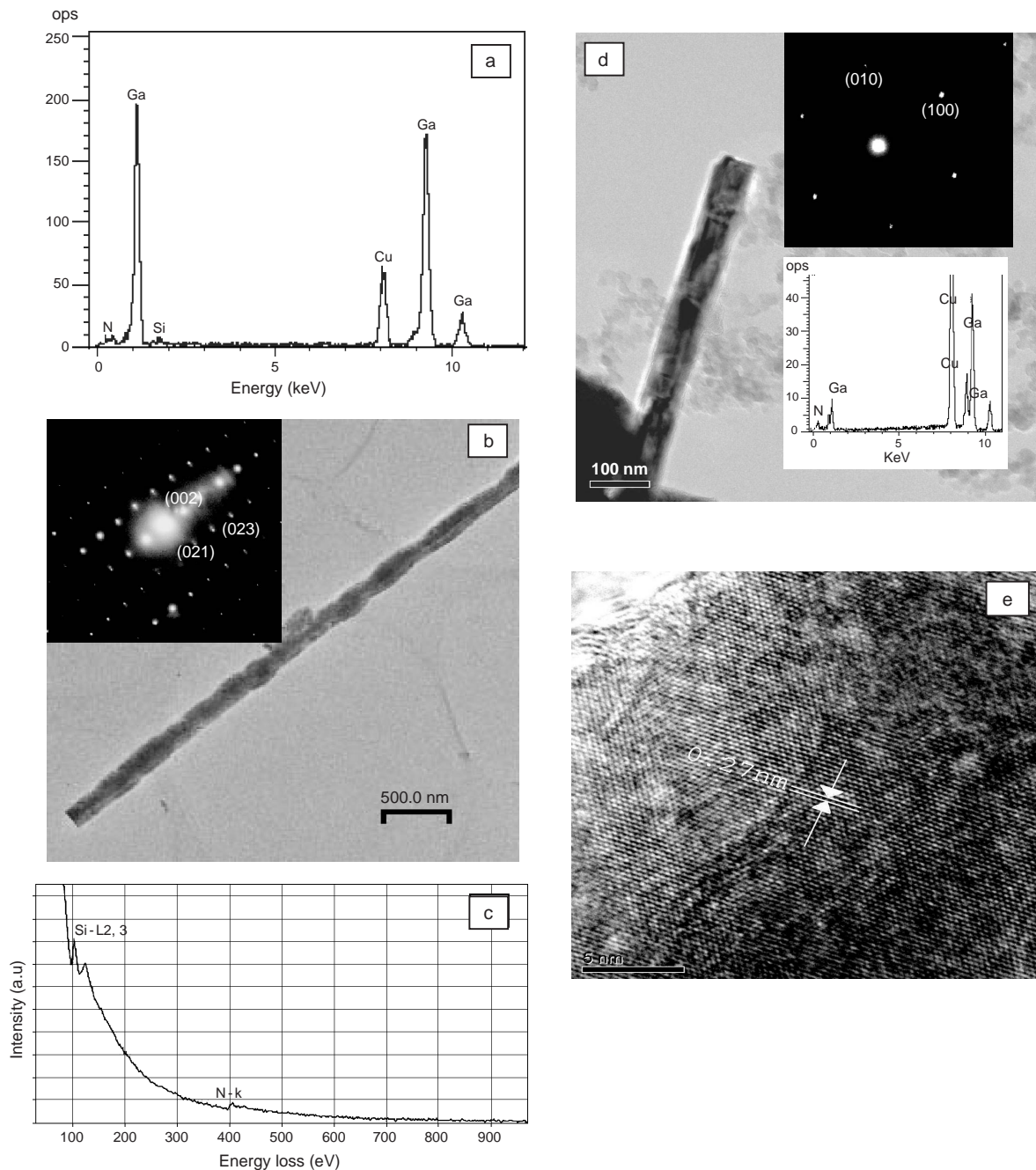


Fig. 4. (a) EDX of the sample A. (b) A typical TEM of the sample A, the inset is SAED. (c) EELS data of the nanowire grown on the substrate. (d) TEM image of the nanowire grown on the substrate B, the upper and lower insets are SAED and EDX, respectively. (e) HRTEM image of the nanowire in (d).

relative to the background are weaker, indicating that the crystallinity of sample B is not so good as that of sample A. In sample B, the peak (101) is the strongest, instead of (002).

Figure 4a shows the energy dispersive X-ray spectroscopy (EDX) analyses. It indicates that sample A consists of Ga, N, and Si, with an atomic ratio of 38.55:60.57:0.88. The atomic ratio of Ga to Si is about 97.8:2.2. Different areas of a single nanowire and dozens of nanowires have been analyzed by EDX attached to

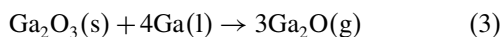
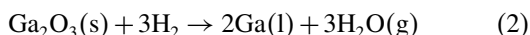
TEM. These results indicate that Si is uniformly contained in GaN nanowires. Figure 4b shows a typical bright-field TEM image of a nanowire. The inset is its selected area electron diffraction (SAED), which can be indexed to a wurtzite hexagonal structure GaN. This result indicates that the nanowire is a single crystal with [001] growth direction. In addition, no second set of diffraction points or irregular points was observed.

The electron energy loss spectra (EELS) data for a nanowire grown on substrate A is shown in Figure 4c.

The nanowire shows three distinct absorption features corresponding to Si-L₂, L₃, and N-K in the range of energy loss from 50 to 900 eV, indicating that Si has been doped into GaN nanowires.

Figure 4d shows a typical bright-field TEM image of the nanowire grown on the substrate B. The diameter of the nanowire is about 70 nm. The upper and lower insets are SAED pattern and EDX analysis, respectively. The EDX analysis indicates that the nanowire consists of Ga and N. The atomic ratio of Ga to N is about 49:51. The SAED pattern can be indexed to single-crystal hexagonal GaN; the [110] direction is parallel to the long axis of the nanowire, indicating that the fast-growth direction is along the [110] direction, which is different from the case of substrate A whose growth direction is along [001]. The lattice spacing of 0.27 nm, as shown in the HRTEM image (Fig. 4e), corresponds to (100) crystal planes of the hexagonal GaN.

There are probably several chemical reactions involved in our method to fabricate GaN based nanowires. According to the thermodynamic data, the Ga₂O₃ cannot directly react with NH₃ since the free energy of reaction is positive ($\Delta G_r = 180-94 \text{ kJ/mol}^{-1}$) in the temperature range 300–1200 °C. Because of the presence of Ar + H₂, Ga₂O₃ will be reduced to Ga through the following reactions:²⁰



Moreover, NH₃ decomposes stepwise to NH₂, NH, H₂, and N₂ at temperature above 800 °C. Hence, H₂ can be assumed to be present in our furnace after the Ar + H₂ was turned off and NH₃ was introduced. As Ga₂O and Ga are much more volatile than Ga₂O₃ at the processing temperature, Ga can be readily transported to substrate A by the carrier gas. From a thermodynamic point of view, Ga can easily etch the surface of silica substrate around 950 °C. The following reaction may occur:²¹



Newly formed Si can dissolve into Ga to form Ga–Si droplets since Si cannot react with SiO₂ below 1100 °C.²² The solubility of Si in Ga is about 5 atom % above 800 °C under vacuum.²³

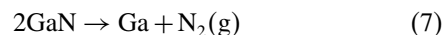
The following reaction occurs:



Reaction 6 might occur either in the vapor or in the Ga–Si droplets. The Ga₂O, NH₃, and GaN dissolve in the liquid alloy droplets of Ga–Si. When the GaN concentration

reaches the saturation level in the Ga–Si droplet, solid GaN will segregate at the droplet–substrate interface. Thus, the Ga–Si droplet acts as a nucleation site for GaN segregation and as a medium to dissolve GaN and Si. Finally, Ga_{1-x}Si_xN nanowires are formed.¹⁸ In this process, the growth mechanism is dominated by vapor–liquid–solid (VLS).²¹

Because the temperature of the substrate A (900–950 °C) is a bit less than the decomposition temperature (above 950 °C) of GaN,^{24,25} some GaN based nanowires are more likely to be unstable and subsequently decompose into Ga and N₂:



Si(s) segregates from Ga. Ga will be carried away by carrier gas and deposited onto substrate B (around 800 °C). From a thermodynamic point of view, reaction 4 is not workable, since the temperature of substrate B is below 900 °C. No silicon source is available. Hence, the following reaction occurs:



In this reaction, partial Ga is probably from reaction 2.



In this process, the growth mechanism is likely to be governed by vapor solid (VS).

Raman scattering is sensitive to microscopic structure, which can provide further information on vibrational states of Ga_{1-x}Si_xN and GaN nanowires. On the other hand, according to band mode and the selection rules, we can also judge its crystalline quality. In terms of the factor group analysis, a single-crystal GaN possesses eight sets of optical phonon modes near the zone center. These modes are classified into Raman ($A_1 + E_1 + 2E_2$), silent ($2B_1$), and infrared active ($A_1 + E_1$). The A_1 and E_1 modes are further split into LO (longitudinal optical) and TO (transverse optical) components. For the sample A, as shown in Figure 5a, first, the four observed Raman-active phonon bands near 136, 527, 563, and 703 cm⁻¹ correspond to E_2 (low), A_1 (TO), E_2 (high), and A_1 (LO) modes, respectively. The frequencies of the first three modes are close to those previously reported on nanowires and bulks,^{26–28} the position of the A_1 (LO) mode is significantly softer. Second, we find that these phonon peaks broaden substantially in the case of the nanowires. Third, the strongest E_2 (high) phonon line reflects the characteristics of the hexagonal crystal phase of the GaN nanowires. Only the allowed modes according to the selected rule are manifested, illustrating that structural defects or internal stress are minimal in the sample. Two additional modes were observed at 419 and 665 cm⁻¹, both of which are not allowed by the C_{6v} space group in first-order Raman scattering at the zone center. The peak at 419 cm⁻¹ can

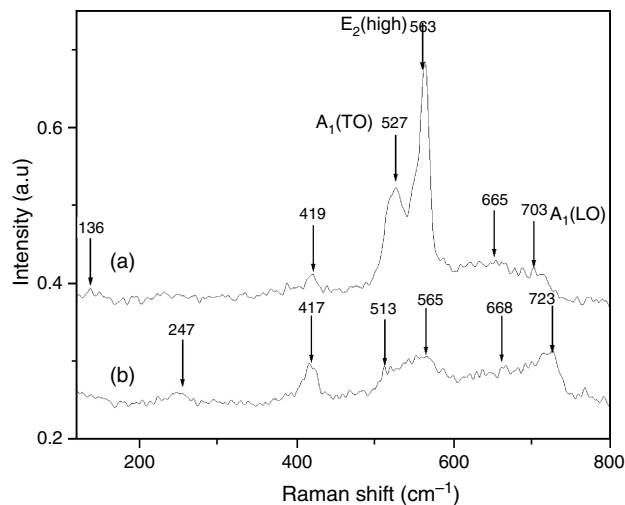


Fig. 5. Raman scattering spectroscopy of the samples A (a) and B (b).

be assigned to the zone-boundary phonon, whereas the peak at 665 cm^{-1} can be indexed into the defect-induced phonon mode. This behavior agrees with the spatial correlation or phonon confinement model, which suggests that phonons in nanometric systems can be confined in space by crystallite boundaries or surface disorders. Consequently, this confinement causes an uncertainty in the wave vector of the phonons, which results in broadening of the Raman features. Similar evidence for the broadening of the Raman bands associated with the phonon confinement effects has been observed in the micro- and nanocrystallite systems, such as Si and GaAs.²⁹

For the sample B, as shown in Figure 5b, the peaks at 513 , 565 , and 723 cm^{-1} are the first-order phonon frequencies of $A_1(\text{TO})$, $E_2(\text{high})$, and $A_1(\text{LO})$, respectively.⁹ The strength of $A_1(\text{LO})$ is almost the same as that of $E_2(\text{high})$, that is, $I_{E_2(\text{high})}/I_{A_1(\text{LO})} \leq 1$, which is contrary to the common observation of a high $I_{E_2(\text{high})}/I_{A_1(\text{LO})}$ ratio. This may be assigned to surface disorder and strong stress in the differently oriented unit cells along the growth.

Apparently, the peaks of both sample A and B were shifted to lower frequency and broadened compared to those of bulk GaN single crystal.^{30–32} The red shifts of the $E_2(\text{high})$, $A_1(\text{LO})$, and $A_1(\text{TO})$ modes are 3, 23, and 5 cm^{-1} , respectively. Gao et al.³³ also found a red shift in the Raman scattering spectrum of Ga_2O_3 nanorods, in the present work; because gallium oxide was used as a starting material and residual oxygen existed in the furnace, the gallium oxide is probably incorporated into GaN nanowires. Accordingly, we also believe that the red shift of GaN nanowires originated from some defects and further investigation is needed.

Figure 6 shows the room temperature (300 K) PL spectra of the Si-doped GaN (Fig. 6a) and undoped GaN nanowires (Fig. 6b). A band-edge emission was observed at 358 nm (3.46 eV) for the $\text{Ga}_{1-x}\text{Si}_x\text{N}$. The well-known defect-induced yellow emission band is not observed,

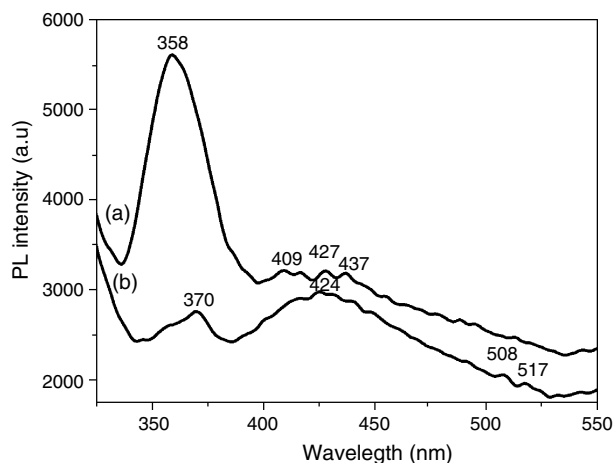


Fig. 6. PL spectra of the samples A (a) and B (b).

indicating high quality of the Si-doped GaN nanowires. A broad emission band around 425 nm (2.92 eV) was also observed, which should be related with defect sites and/or surface states. In PL spectra of GaN doped with Mn or Mg, similar bands at 425 nm (2.92 eV) have been observed,^{34,35} indicating that this band may arise from the defect sites. For GaN nanowires, band-edge emission was observed at 370 nm (3.37 eV) with much weaker intensity, whereas the 425-nm (2.92 eV) emission becomes much stronger, indicating that defect concentration is higher in the GaN nanowire.

The band-edge emission of the Si-doped GaN nanowire is blue-shifted from that of the GaN nanowires by $\sim 12\text{ nm}$ ($\sim 90\text{ meV}$). Although a significant fraction of the Si-doped GaN nanowires have diameters less than that of GaN, quantum confinement may not be responsible for the blue shift, since the diameters of the nanowires are much larger than the exciton Bohr radius of the bulk GaN (2.8 nm). The blue shift may also arise from the Si dopant. Recent research on Si-doped GaN film has attributed the shift of the band gap to the shifts of both conduction and valence bands.³⁶ The band-edge emission showed non-monotonic behavior: the position decreases initially as the dopant concentration increases and showed an increase by further increase in doping. A more detailed PL study is in progress and will be published in a separate paper.

In summary, a bulk quantity of Si-doped GaN and undoped GaN nanowires has been successfully synthesized via conventional CVD method in the presence of a suitable gas atmosphere. Several techniques were employed to analyze the as-prepared nanowires, indicating that the Si-doped GaN nanowires have a single-crystal hexagonal wurtzite structure along with 2.2 atom % Si. The broadening and the lower frequency shift of Raman peaks are probably attributed to surface disorder and the stress. The blue shift of band-gap emission of Si-doped GaN nanowires relative to that of GaN nanowires is due to doping impurity Si.

Acknowledgments: This project was supported in part by the electron Spin Science Center (eSSC) funded by Korea Science and Engineering foundation (KOSEF) and BK 21 project in 2004 funded by Korea Research foundation.

References and Notes

1. G. Fasol, *Science* 272, 1751 (1996).
2. S. Nakamura, *Science* 281, 956 (1998).
3. H. Morkoc and S. N. Mohanmmad, *Science* 267, 51 (1995).
4. W. Han, S. Fan, Q. Li, and Y. Hu, *Science* 277, 1287 (1997).
5. F. A. Ponce and D. P. Bour, *Nature* 386, 351 (1997).
6. W. Shi, Y. Zheng, N. Wang, C. Lee, and S. Lee, *Adv. Mater.* 13, 591 (2001).
7. X. Duan and C. Lieber, *J. Am. Chem. Soc.* 122, 188 (2000).
8. C. Chen and C. Yeh, *Adv. Mater.* 12, 738 (2000).
9. M. He, I. Minus, P. Zhou, S. Mohammed, J. Halpern, R. Jacobs, W. Sarney, L. Salamanca-Riba, and R. Vispute, *Appl. Phys. Lett.* 77, 3731 (2000).
10. C. C. Chen, C. H. Yeh, C. H. Chen, M. Yu, H. Liu, J. Wu, K. H. Chen, L. C. Chen, J. Peng, and Y. F. Chen, *J. Am. Chem. Soc.* 123, 2791 (2001).
11. X. Chen, J. Li, Y. Cao, Y. Lan, H. Li, M. He, C. Wang, Z. Zhang, and Z. Qiao, *Adv. Mater.* 12, 1432 (2000).
12. J. R. Kim, H. So, J. Park, J. J. Kim, J. Kim, C. Lee, and S. Lyu, *Appl. Phys. Lett.* 80, 3548 (2002).
13. K. Chang and J. Wu, *J. Phys. Chem. B* 106, 7796 (2002).
14. W. Han, P. Redlich, F. Ernst, and M. Rühle, *Appl. Phys. Lett.* 76, 652 (2000).
15. W. Han, S. Fan, Q. Li, and Y. Hu, *Science* 277, 1287 (1997).
16. G. Chen, L. Zhang, Y. Zhu, G. Fei, L. Li, C. Mo, and Y. Mao, *Appl. Phys. Lett.* 75, 2455 (1999).
17. F. L. Deepak, P. V. Vanitha, A. Govindaraj, and C. N. R. Rao, *Chem. Phys. Lett.* 374, 314 (2003).
18. J. Liu, X. M. Meng, Y. Jiang, C. S. Lee, I. Bello, and S. T. Lee *Appl. Phys. Lett.* 83, 4241 (2003).
19. J. Neugebauer and C. G. van de Walle, *Phys. Rev. B* 57, 2033 (1998).
20. Z. Lan, C. Liang, C. Hsu, C. Wu, H. Lin, S. Dhara, K. Chen, L. Chen, and C. Chen, *Adv. Funct. Mater.* 14, 233 (2004).
21. C. C. Tang, S. S. Fan, M. L. Chapelle, and P. Li, *Chem. Phys. Lett.* 333, 12 (2001).
22. R. B. Heslop and P. L. Robinson, *Inorganic Chemistry*, Elsevier, New York (1960), p. 287.
23. B. Girault, F. Chevrier, A. Joullie, and G. Bougnot, *J. Cryst. Growth* 37, 169 (1977).
24. H. W. Choi, M. A. Rana, S. J. Chua, T. Osipowicz, and J. S. Pan, *Semicond. Sci. Technol.* 17, 1223 (2002).
25. J. Y. Li, X. L. Chen, Z. Y. Qiao, Y. G. Cao, and Y. C. Lan, *J. Cryst. Growth* 213, 408 (2000).
26. T. Azuhata, T. Sota, K. Suzuki, and S. Nakamura, *J. Phys.: Condens. Matter* 7, L129 (1995).
27. L. Filippidis, H. Siegle, A. Hoffmann, C. Thomsen, K. Karch, and F. Bechstedt, *Phys. Status Solidi B* 198, 621 (1996).
28. V. Y. Davydov, Y. E. Kitaev, I. N. Goncharuk, A. N. Smirnov, J. Graul, O. Semchinova, D. Uffmann, M. B. Smirnov, A. P. Mirgorodsky, and R. A. Evarestov, *Phys. Rev. B* 58, 12 899 (1998).
29. X. S. Zhao, Y. R. Ge, J. Schroeder, and P. D. Persans, *Appl. Phys. Lett.* 65, 2033 (1994).
30. W. J. Wang, Y. T. Song, W. X. Yuan, Y. G. Cao, X. Wu, and X. L. Chen, *Appl. Phys. A* 78, 29 (2004).
31. G. Wei, J. Zi, K. Zhang, and X. Xie, *J. Appl. Phys.* 82, 4693 (1997).
32. Y. G. Cao, X. L. Chen, Y. C. Lan, Y. P. Xu, T. Xu, and J. K. Ling, *J. Mater. Res.* 15, 267 (2000).
33. Y. H. Gao, Y. Bando, T. Sato, and Y. F. Zhang, *Appl. Phys. Lett.* 81, 2267 (2002).
34. M. Leroux, N. Grandjean, B. Beaumont, G. Nataf, F. Sémond, J. Massies, and P. Gibart, *J. Appl. Phys.* 86, 3721 (1999).
35. J. M. Baik, J. L. Lee, Y. Shon, and T. W. Kang, *J. Appl. Phys.* 93, 9024 (2003).
36. A. F. D. Silva, C. M. Araujo, B. E. Sernelius, and C. Persson, *J. Phys.: Condens. Matter* 13, 8891 (2001).

Received: 27 August 2004. Revised/Accepted: 16 November 2004.